Involvement of the Src-cortactin pathway in podosome formation and turnover during polarization of cultured osteoclasts

Chen Luxenburg[1], J. Thomas Parsons[2], Lia Addadi[3] and Benjamin Geiger[1,*]

[1]Department of Molecular Cell Biology, Weizmann Institute of Science, Rehovot 76100, Israel
[2]Department of Microbiology, University of Virginia Health System, Charlottesville, VA 22908, USA
[3]Structural Biology, Weizmann Institute of Science, Rehovot 76100, Israel
*Author for correspondence (e-mail: benny.geiger@weizmann.ac.il)

Accepted 20 September 2006
Journal of Cell Science 119, 4878-4888 Published by The Company of Biologists 2006
doi:10.1242/jcs.03271

Summary

Osteoclasts are large, multinucleated cells that adhere to bone via podosomes, and degrade it. During osteoclast polarization, podosomes undergo reorganization from a scattered distribution, through the formation of clusters and ring super-structures, to the assembly of a sealing zone at the cell periphery. In the present study, we demonstrate that the levels of podosome-associated actin, and its reorganization in cultured osteoclasts, radically increase upon formation of podosome rings. At the peripheral ring, actin levels and dynamic reorganization were high, whereas paxillin, associated with the same adhesion super-structure, remained relatively stable. These dynamic changes were regulated by the tyrosine kinase pp60$^{c\text{-}Src}$, whose scaffolding activity supported the assembly of immature stationary podosomes; its catalytic activity was essential for podosome maturation and turnover. The enhanced dynamic reorganization of podosomes during osteoclast polarization was inversely related to the local levels of tyrosine phosphorylation of the Src substrate, cortactin. Furthermore, overexpression of cortactin, mutated at its major Src phosphorylation sites, enhanced actin turnover, suggesting that podosome dynamics in polarizing osteoclasts are attributable to the downregulation of cortactin activity by its Src-dependent phosphorylation.

Supplementary material available online at
http://jcs.biologists.org/cgi/content/full/119/23/4878/DC1

Key words: Osteoclast, Podosomes, Src, Cortactin

Introduction

Osteoclasts are large, multinucleated cells whose primary function is bone resorption. This process is regulated at multiple levels, including the proliferation and homing of osteoclast progenitors and their fusion into multinucleated cells (reviewed by Teitelbaum, 2000). Upon identification of appropriate resorption sites, osteoclasts reorganize their small matrix adhesions – podosomes – into a circular adhesion structure at the cell periphery known as the 'sealing zone', and secrete protons and lysosomal enzymes into the space between the cell and the bone surface (Nesbitt and Horton, 1997; Salo et al., 1997). These structures form readily on bone surfaces; similar organization of podosome super-structures was observed in cells grown on standard tissue culture surfaces (Calle et al., 2004; Lakkakorpi et al., 1993; Zambonin-Zallone et al., 1988).

Podosomes are small (~1 μm in diameter) dot-like adhesion structures found in osteoclasts, macrophages, dendritic cells and several types of transformed cells (reviewed by Linder and Aepfelbacher, 2003). They consist of an actin core surrounded by a 'ring domain' containing αvβ3 integrin and several focal adhesion proteins (Zambonin-Zallone et al., 1989). The actin core consists of a bundle of F-actin running perpendicular to the substratum, as well as several actin-associated proteins such as cortactin (Hiura et al., 1995), Wiskott-Aldrich Syndrome protein (WASP) (Calle et al., 2004), actin-related protein complex 2/3 (Arp2/3) (Hurst et al., 2004), gelsolin (Chellaiah et al., 2000) and dynamin (Ochoa et al., 2000). It has been proposed that these proteins acting in concert to regulate actin organization and dynamics at this site.

Previous studies (Destaing et al., 2003) have shown that podosomes in cultured osteoclasts can assemble into large super-structures such as clusters or rings, and eventually form a stable peripheral belt. The belt can further condense, giving rise to a ~4-μm-wide actin domain flanked by outer and inner plaque domains containing integrins and focal adhesion proteins. This structure resembles the sealing zone found in bone-resorbing osteoclasts (Lakkakorpi et al., 1993), and will therefore be referred to herein as a 'sealing-zone-like' (SZL) structure. The formation of podosomes, their dynamic properties, and their step-wise assembly into a SZL structure are essential for the resorptive activity of these cells.

One of the major mechanisms involved in the regulation of podosome development is tyrosine phosphorylation by the cytoplasmic kinase pp60$^{c\text{-}Src}$ (Src). This enzyme is essential for osteoclast activity in vivo, because Src knockout mice suffer from severe osteopetrosis caused by deficient osteoclast activity (Soriano et al., 1991). Osteoclasts derived from such

mice cannot adhere and spread properly, and fail to give rise to mature sealing zones when plated on bone, or to SZL structures when plated on tissue culture dishes (Lakkakorpi et al., 2001). Excessive Src activity (e.g. owing to the expression of an oncogenic Src mutant, v-Src), on the other hand, perturbs focal adhesions and induces podosome formation in a variety of cell types (Tarone et al., 1985). However, despite the clear indication that Src is involved in osteoclast adhesion-mediated signaling (Miyazaki et al., 2004; Sanjay et al., 2001) and podosome assembly (Tarone et al., 1985), the underlying mechanisms and the nature of the Src targets involved in podosome dynamics are still poorly understood.

Recently we have shown that the molecular composition of podosomes changes dramatically during osteoclast polarization: local levels of actin and plaque proteins increase, while tyrosine phosphorylation levels decrease (Luxenburg et al., 2006). However, the nature of the phosphorylated target(s) and the subsequent effects on podosome dynamics during osteoclast polarization has yet to be clarified.

In the present study, we have addressed the involvement of Src, as well as the Src target protein cortactin, in podosome dynamics during osteoclast polarization. We demonstrate that actin associated with rings of podosomes and SZL structures is considerably more dynamic (by a factor of about two to three) than actin in clustered podosomes. However, the paxillin-rich plaque associated with the SZL structure is considerably more stable. Osteoclasts expressing a constitutively active Src are polarized and display ectopic rings with high turnover, yet they fail to form a stable, mature, SZL structure. By contrast, osteoclasts expressing a dominant-negative Src, lacking the kinase domain, do not polarize, and their podosomes are nearly stationary.

We further show that the actin-nucleating protein cortactin, which is a known Src substrate (Wu et al., 1991), is highly tyrosine phosphorylated in clustered podosomes, but not in podosome rings or in SZL structures. This finding is consistent with the notion that the Src-mediated phosphorylation of cortactin reduces its capacity to enhance actin polymerization (Huang et al., 1997a; Huang et al., 1997b; Martinez-Quiles et al., 2004). Moreover, we show that overexpression of a non-phosphorylatable cortactin mutant increases the turnover of podosomes, without inducing ring formation.

Results

Dynamics of podosome reorganization during osteoclast polarization

To study podosome dynamics, cultured RAW cells stably expressing GFP-actin, or transiently expressing YFP-paxillin, were induced to differentiate into osteoclasts. Four sequential patterns of podosome organization were observed in these cells: (1) individual podosomes scattered throughout the ventral cell surface. These structures typically consisted of an actin-rich core (Fig. 1A, ind pod/cluster, marked with an arrow) and a paxillin-rich ring domain surrounding the core (Fig. 1C, ind pod/cluster, marked with an arrow). (2) Podosome clusters (Fig. 1A,C, ind pod/cluster) formed following accumulation or

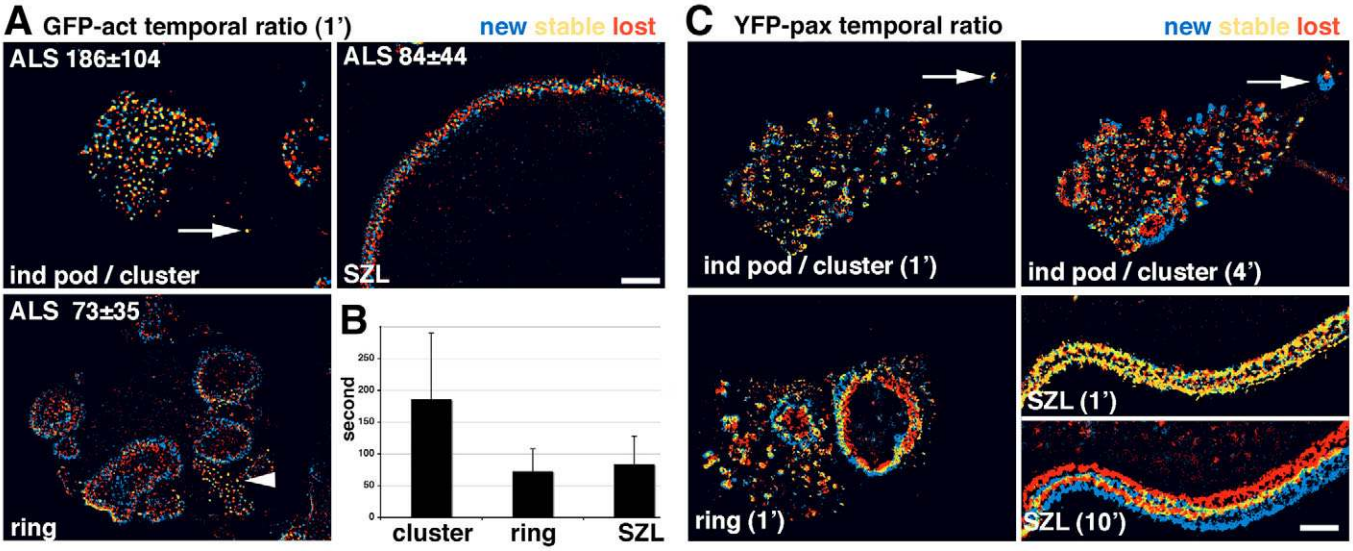

Fig. 1. Dynamic development of podosome organization during osteoclast polarization. RAW cells, either stably expressing GFP-actin or transiently transfected with YFP-paxillin, were induced to differentiate into osteoclasts and were recorded at 15-second intervals by time-lapse microscopy. (A) Temporal ratio images of GFP-actin. Four distinct, consecutive stages of podosome organization are shown: Individual podosomes (ind pod/cluster) (see arrow); clusters; rings; and sealing-zone-like (SZL) structures. Temporal ratio images indicate new podosomes (~1-minute old) in blue, podosomes that disappeared within the same minute of recording, in red, and more stable podosomes in yellow (see color legend in Figure). Actin reorganization in individual podosomes and clusters is slower than in ring and SZL structures. Note that clustered podosomes are less dynamic than ring podosomes within the same cell (ring, marked with arrowhead). (B) The quantitative data represent the average podosome life span (ALS) ± s.d., based on GFP-actin movies of five cells for every structure, obtained in three independent experiments. A total of 240 podosomes were examined for clusters and SZL structures; 220 podosomes were examined for rings. Statistical analysis based on the Student's *t*-test showed significant differences between cluster and ring structures ($P<5\times10^{-41}$), and cluster and SZL structures ($P<5\times10^{-41}$). (C) Temporal ratio image of YFP-paxillin. Paxillin ring domains in individual podosomes and clusters appeared less dynamic than in rings. Note the transition from an individual podosome to a cluster (ind pod/cluster 1' and 4', arrow). The SZL structure is a stable, continuous structure. The apparent sliding of the SZL structure was evident in the 10' temporal ratio image. Bars, 10 μm.

'proliferation' of individual podosomes (Fig. 1C, ind pod/cluster 1' and 4', marked with arrows). (3) Podosome rings extending toward the cell periphery (Fig. 1A,C, ring). (4) SZL structures consisting of a dynamic actin belt (Fig. 1A, SZL) flanked by stable paxillin belts at the periphery of the cell (Fig. 1C, SZL 1') (see also supplementary material Movies 1 and 2).

Temporal ratio analysis of GFP-actin movies revealed an increase in actin-core dynamics (Fig. 1A) upon the transition from clusters to rings, as manifested by the blue and red pixels dominating the image, and indicative of high turnover. A similar analysis of YFP-paxillin movies showed an increase in plaque reorganization upon cluster-ring transition, followed by stabilization upon maturation of the SZL structure (Fig. 1C).

Calculation of the apparent life span of GFP-actin in podosomes (namely, the average length of time from the first appearance of a new podosome, until its dissociation; Fig. 1B) was based on time-lapse movies, and indicates that actin in clustered podosomes has an apparent life span of 186±104 seconds. Upon transition into rings, a two- to threefold increase in the rate of actin reorganization was measured, reaching an average life span of 73±35 seconds. In SZL structures, the average life span of actin-rich structures was 84±44 seconds (for statistical evaluation, see legend to Fig. 1). The average life span of individual podosomes was not determined; because these structures are relatively rare and robust, statistical analysis could not be obtained. It was more difficult to quantify the dynamic reorganization of paxillin in the podosome ring domain because individual structures could not be readily resolved. However, in sparse clusters, the life span of the plaque was comparable with that of the associated actin.

The overall dynamic reorganization in podosomes, visualized by time-lapse video microscopy, included instances of podosome fusion and fission (Fig. 2A and B, respectively) similar to those reported for macrophage-associated podosomes (Evans et al., 2003). Fusion or fission events were noted in ~30% of cluster podosomes and ~50% of podosomes associated with SZL structures. Time-lapse, two-color movies of GFP-pax and Cherry-act indicate that fusion or fission events occur at the level of both the actin-core and the ring domain, though changes in the local actin organization, apparently precede the changes in the paxillin-containing ring (see supplementary material Fig. S1). We also noted an apparent lateral 'sliding' of podosomes (Fig. 2C) as well as the sliding of the entire SZL structure (Fig. 1C, SZL 10').

To quantify these dynamic events, we used an autocorrelation analysis. For this, we segmented podosomes organized in clusters or SZL structures in the first frame of each movie; their subcellular location, area and intensity were then correlated with the fluorescence of the same pixels in each consecutive frame. An autocorrelation value of one indicated no change, and a value of zero indicated complete dissociation or translocation of the structure. The rate at which the correlation value declined corresponded to the dynamic reorganization of podosomes, including their turnover, fusion, fission, sliding and intensity changes. The correlation decay constant corresponded to the time it took for the correlation to

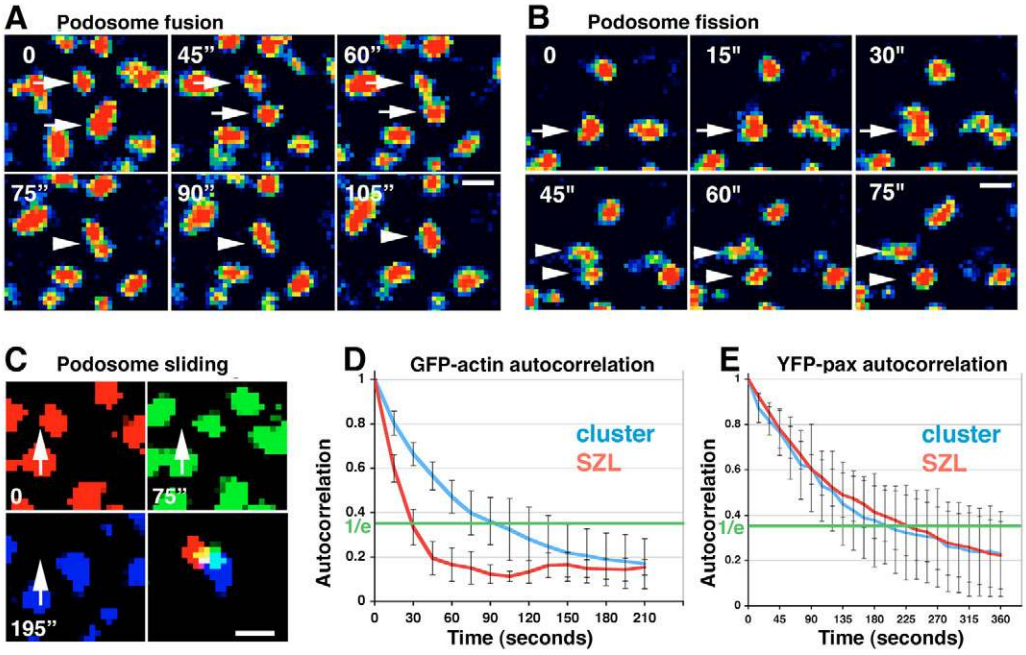

Fig. 2. Podosome fusion, fission and sliding. (A) Podosome fusion within a cluster. Frames from a GFP-actin movie show two neighboring podosomes (0-60", arrows) that approach each other and fuse (75-105", arrowheads). (B) Podosome fission within a cluster. Frames from a GFP-actin movie show podosome splitting (0-30", arrows), creating two daughter podosomes (45"-75", arrowheads). (C) Apparent sliding motion of a podosome within a cluster. Frames from a GFP-actin movie are shown. Podosomes recorded at three time points are marked with different artificial colors (arrows indicate the original localization of the podosome). Time-lapse movies of cells expressing (D) GFP-actin or (E) YFP-paxillin analyzed by temporal autocorrelation techniques. The green line represents the correlation decay time constant (1/e). Five cells were analyzed for every podosome pattern. The blue line represents cluster podosomes and the red line represents SZL structure podosomes. (D) GFP-actin cluster podosomes decayed after 105 seconds; GFP-actin SZL structure decayed after 30 seconds. (E) YFP-paxillin in the cluster decayed after 195 seconds; YFP-paxillin in the SZL structure decayed after 225 seconds. Bars, 1 μm.

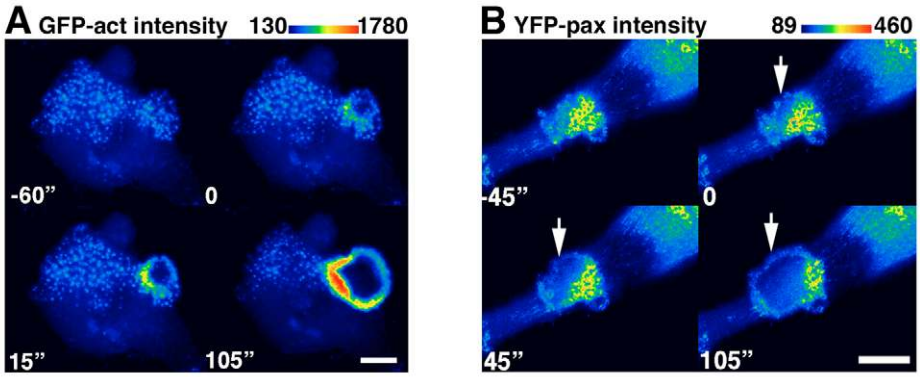

Fig. 3. Changes in the levels of podosome-associated actin and paxillin during cluster-ring transition. RAW cells expressing GFP-actin or YFP-paxillin were induced to differentiate into osteoclasts, and recorded at 15-second intervals by time-lapse video microscopy. Frames are presented in an intensity spectrum scale. A negative time point indicates seconds before the transition. Time point 0 indicates the beginning of cluster-ring transition. (A) An increase in GFP-actin intensity (about tenfold) is evident during cluster-ring transition (0-105"). (B) A slight decrease in YFP-paxillin intensity is noted during cluster-ring transition (0-105"). Arrows indicate the ring. Bars, 10 μm.

reach a value of 0.37 (1/e). The average time constant for cluster-associated GFP-actin was 105 seconds, compared with 30 seconds for SZL structures (Fig. 2D). Paxillin associated with these structures was considerably more stable than actin, with time constants of 195 seconds and 225 seconds, respectively (Fig. 2D).

It is noteworthy that, concomitantly with the transition to a more dynamic state, the transformation of a podosome cluster into a ring was accompanied by an ~tenfold increase in local GFP-actin intensity (Fig. 3A). Image filtration suggests that the increase in GFP-actin intensity was related to an increase in both the actin core and the surrounding 'actin cloud'. Similar differences in GFP-actin or phalloidin staining intensity were also noted between the SZL structure and cluster podosomes in the lamella of the same cell (see Fig. 4, act, and Fig. 7A, act). Unlike the increase in actin intensity, we noted a moderate decrease (15%) in the intensity of YFP-paxillin upon cluster-to-ring transition (Fig. 2B). However, the intensity of paxillin associated with the SZL region was about tenfold higher than the intensity of paxillin associated with cluster podosomes within the same cell, based on YFP-paxillin or staining for the endogenous protein (data not shown). We conclude that during the assembly of the SZL structure, actin dynamics increase two- to threefold, whereas paxillin associated with the same superstructure stabilizes.

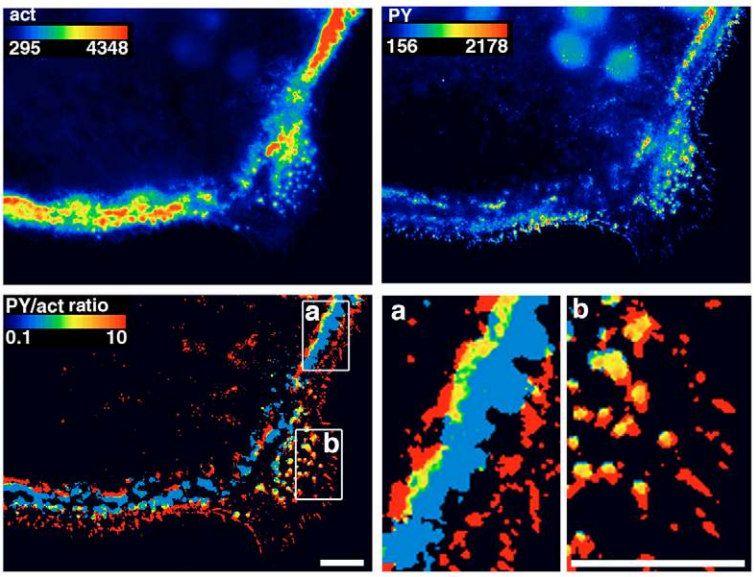

Fig. 4. Differential tyrosine phosphorylation of podosomes during osteoclast polarization. RAW cells were induced to differentiate, and then fixed and double-stained for actin and phosphotyrosine (PY). Actin and PY are shown in an intensity spectrum scale. Ratio images (PY/act ratio) demonstrate tyrosine phosphorylation of the entire actin domain of clustered podosomes (b) whereas in the SZL structure (a) tyrosine phosphorylation is predominantly associated with the plaque domain. Bars, 10 μm.

The role of Src-induced tyrosine phosphorylation in podosome assembly and dynamics

Tyrosine-specific phosphorylation of podosome components has been implicated in the regulation of podosome development (Tarone et al., 1985). We previously demonstrated in primary osteoclasts that the transition from clustered podosomes to rings and SZL structures is accompanied by a decrease in phosphotyrosine (Luxenburg et al., 2006). However, the nature of the phosphorylated molecule(s) has not yet been clarified.

To investigate the mechanisms underlying the effects of tyrosine phosphorylation in our experimental model, RAW cells were induced to differentiate, then fixed and immunolabeled for actin and phosphorylated tyrosine (PY) (Fig. 4). Quantitative fluorescence microscopy indicated that podosomes at all stages of development were tyrosine phosphorylated; yet the labeling intensity was found to be higher in podosome clusters than in rings and SZL structures (Fig. 4, PY). Phosphorylation of individual and clustered podosomes was associated with both the actin-rich core and the surrounding ring domain. In rings of podosomes and SZL structures, podosome phosphorylation was predominantly co-localized with the plaque structure flanking the central actin belt, whereas phosphorylation along the actin-rich core was reduced (Fig. 4 PY/act ratio). In view of the involvement of Src in osteoclast function (Horne et al., 1992; Miyazaki et al., 2004; Sanjay et al., 2001; Soriano et al., 1991), we investigated the involvement of Src catalytic activity in podosome development and dynamics. RAW cells stably

expressing GFP-actin were infected with retroviral vectors encoding either a constitutively active Src (SrcY527F) or a dominant-negative mutant lacking the kinase domain (Src251) (Kaplan et al., 1995) (see supplementary material Movies 3-5). The expression levels of exogenous and endogenous Src in the stable cell lines were assessed by western blot analysis (supplementary material Fig. S2A). Both SrcY527F- and Src251-expressing osteoclasts showed a ~60% decrease in endogenous Src compared with control cells. Moreover, the level of expression of Src251 was 30% higher than that of the endogenous, WT Src. (SrcY527F cannot be discerned from the endogenous Src in such an analysis.) To confirm that the phenotypes described below did not represent clonal variability, we confirmed the dynamic behavior in transiently transfected cells.

Temporal ratio images derived from time-lapse movies of GFP-actin-expressing cells (Fig. 5) show, in a control cell, a well-organized and dynamic SZL structure at the cell periphery, with nearly no podosomes located in the central part of the cell (Fig. 5, control). Overexpression of the deregulated SrcY527F mutant resulted in the formation of polarized osteoclasts with poorly organized SZL structures (Fig. 5, SrcY527F). The SZL structures in these cells displayed extremely rapid turnover. The average life span of actin cores in the mutant was 52±25 seconds, compared with 84±44 seconds in control cells. Moreover, cells overexpressing SrcY527F developed numerous ectopic podosomes, located at the cell center. The average life span of these podosomes was 31±15 seconds. The average number of podosomes in SrcY527F was 2.7-fold greater than that found in polarized control cells (supplementary material Fig. S2B).

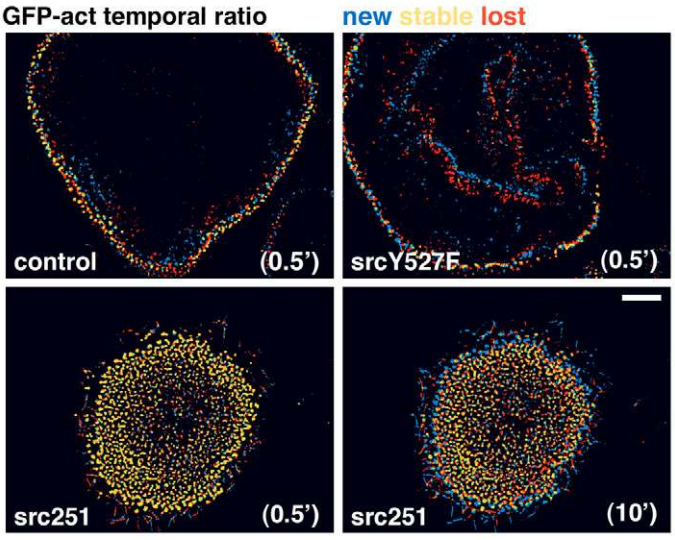

Fig. 5. Effect of modulation of Src activity on podosome organization and dynamics. Temporal ratio imaging of GFP-actin, based on time-lapse microscopy of osteoclasts expressing GFP-actin (control); co-expressing GFP-actin and SrcY527F (SrcY527F); or co-expressing or GFP-actin and Src251 (Src251). Notice the elevated rate of podosome turnover and formation of ectopic podosomes in the SrcY527F-expressing cells, and the predominance of stationary podosomes in the Src251-expressing cells (0.5' and 10'). The calculated average podosome life span (± s.d.) is 52±25 seconds in SZL structures of SrcY527F cells, and 31±15 seconds in the ectopic podosomes of the same cells. The life span of the dynamic podosomes in Src251-expressing osteoclasts was 528±334 seconds. These data were based on measurements taken in five cells, with >200 podosomes for each cell type. Bar, 10 μm.

Overexpression of the dominant-negative Src251 mutant (Fig. 5, Src251 0.5' and 10') resulted in the inhibition of both cell spreading and ring formation: ~25% of the podosomes in these cells failed to turn over after 30 minutes. The average life span of podosomes that did turn over was 528±334 seconds, leading to an accumulation of podosomes throughout the entire ventral membrane (Fig. 5, Src251 10'). On average, Src251 cells had almost three times as many podosomes than non-polarized control cells (cells with individual and cluster podosomes) (supplementary material Fig. S2B). Expression of a truncated mutant (i.e. Src251) in which the SH2 domain was inactivated by mutating Arg175 to Ala, did not exert these effects (data not shown).

To examine the organization of the podosome ring domains in cells expressing the Src mutants, cells were induced to differentiate, then fixed and double-immunostained for vinculin and actin. In control cells, vinculin-containing ring domains surrounded the actin cores (Fig. 6A, control, insert a). In the SZL structures, vinculin flanked the actin belt at the cell periphery, giving rise to the characteristic double ring structure (Fig. 6A, control, insert b). Expression of SrcY527F prevented the formation of the double ring structure at the cell periphery; furthermore, vinculin appeared disorganized, displaying considerable overlap with actin (Fig. 6A, SrcY527F). Vinculin associated with the inner, ectopic podosomes was even less organized, and large amounts of vinculin were diffusely distributed throughout the cytoplasm. Osteoclasts overexpressing Src251 formed abnormal ring domains, which failed to mature and fully encircle the actin core (Fig. 6A, Src251). SZL structures were not detected in these cells, even when the cells were allowed to differentiate for a longer period of time.

To obtain further insights into the role of Src in podosome development, we localized Src (supplementary material Fig. S3) and active Src (Src pY418) (Fig. 6B) in untreated osteoclasts, as well as in osteoclasts overexpressing the different Src mutants. Osteoclasts expressed high levels of endogenous Src, which were localized throughout the cytoplasm, including the perinuclear area, whereas only low levels of Src were associated with the SZL structure (supplementary material Fig. S3A). Src pY418 distribution was more restricted (Fig. 6B), localizing in an inner belt along the actin peripheral belt (Fig. 6B, control). Occasionally, a double belt was observed (data not shown). A similar distribution of Src pY418 was noted in SrcY527F-expressing cells (Fig. 6B, SrcY527F). In cells expressing Src251, active Src was detected next to the actin cores (Fig. 6B, Src251) similar to cluster podosomes in control cells (data not shown). In Src251, unlike control or SrcY527F osteoclasts, intense Src labeling was associated with each and every actin core (supplementary material Fig. S3A). To assess the three-dimensional relationships of Src251 and the actin core, the transfected cells were subjected to two-color confocal microscopy, followed by 3D image reconstruction. *X-Z* images from such series show that the two proteins co-localize thorough the entire actin core bundle (supplementary material Fig. S3B).

We conclude that actin turnover in podosomes is inversely

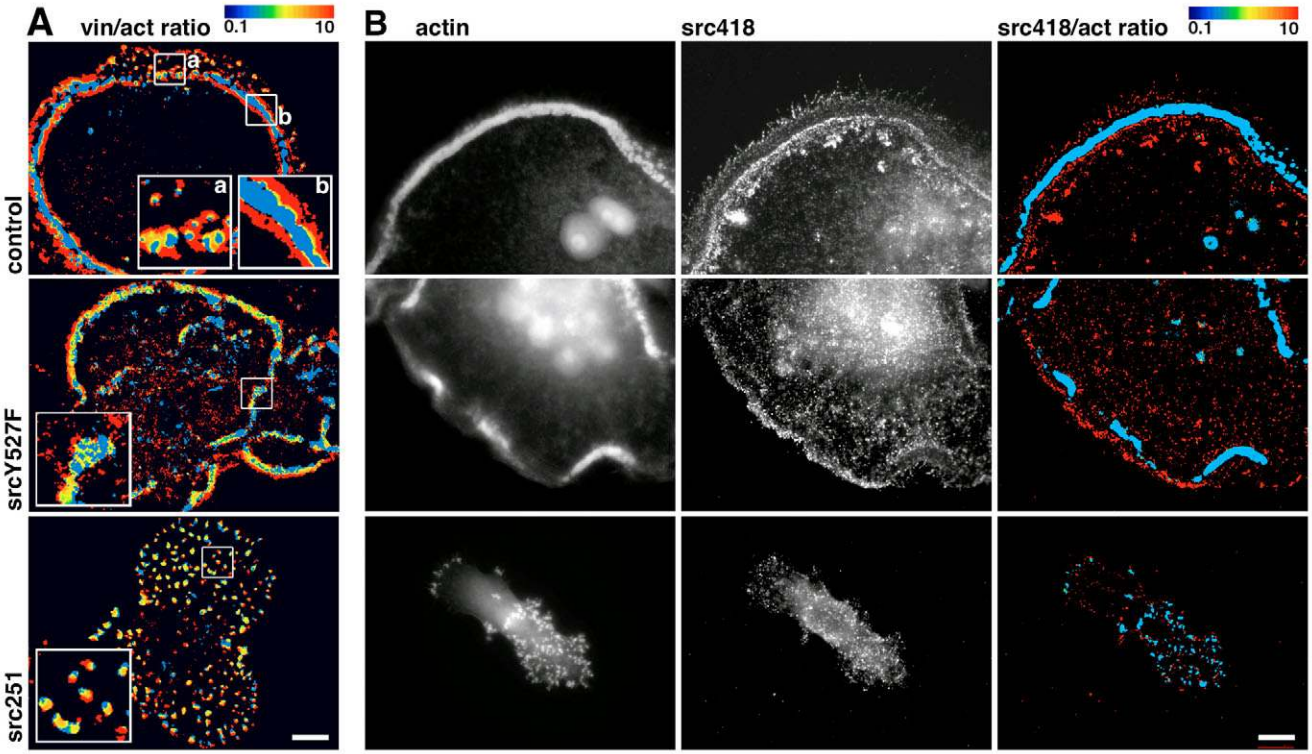

Fig. 6. Src catalytic activity affects podosome development. Osteoclasts derived from RAW cells expressing GFP-actin (control) or co-expressing GFP-actin and SrcY527F (SrcY527F), or GFP-actin and Src251 (Src251), were fixed and double-stained (A) for vinculin and actin, or (B) for Src pY418 and actin. (A) The vinculin/actin ratio indicates a typical double ring structure in control cells. Notice the poorly organized SZL structure in the SrcY527F cell and podosomes with incomplete ring domains, organized in clusters, in the Src251-expressing cells. (B) High levels of Src pY418 (src418) in the inner belt surround control and SrcY527F cells, and surround podosomes in Src251 cells. Bars, 10 μm.

related to their tyrosine phosphorylation. Src scaffolding activity is sufficient to induce the formation of stationary clustered podosomes, while its kinase activity is essential for the proper assembly of the podosome ring domain, podosome maturation into rings, and their dynamic turnover.

The involvement of cortactin phosphorylation in the regulation of podosome dynamics

The observation that modulation of Src activity affects podosome dynamics implies that specific Src targets, whose activity is differentially regulated by phosphorylation, are involved in this process. In this study, we explored the possibility that the effect of Src on podosome dynamics could be mediated by the Src target protein cortactin (Wu and Parsons, 1993; Wu et al., 1991). Src phosphorylates cortactin sequentially on three tyrosine residues, Y421, Y466 and Y482 (Head et al., 2003; Huang et al., 1998); phosphorylation on Y421 is required for phosphorylation of the additional tyrosines (Head et al., 2003), apparently affecting its actin-nucleating activity (Huang et al., 1998; Huang et al., 1997a; Martinez-Quiles et al., 2004). Knockdown of cortactin led to complete loss of podosomes in both osteoclasts (Tehrani et al., 2006) and in smooth muscle cells (Zhou et al., 2005). However, the role of cortactin tyrosine phosphorylation in podosome dynamics is poorly understood.

To explore this issue, RAW osteoclasts were fixed and triple-labeled for F-actin, cortactin and phospho-cortactin (pY421). Like actin, cortactin is distributed throughout the cytoplasm, particularly in the actin cores and 'actin clouds' surrounding all types of podosomes (Fig. 7A, compare actin with cortactin, and notice the co-localization in the cor/act ratio). Phospho-cortactin distribution, on the other hand, was more restricted (Fig. 7A, cor pY421), indicating that although cortactin associated with the actin core in clustered podosomes was highly phosphorylated, ring- and SZL structure-associated cortactin was not (Fig. 6A, cor pY421/cor ratio). Cortactin phosphorylation in the SZL structures is predominantly associated with the actin cloud (supplementary material Fig. S4). Similar differences in cortactin phosphorylation were detected in primary osteoclast-like cells (supplementary material Fig. S5A,B).

To relate the state of cortactin phosphorylation to podosome dynamics in different activation states, RAW cells overexpressing SrcY527F or Src251 were induced to differentiate, and then fixed and triple labeled for actin, cortactin and cortactin pY421. A comparison of actin and cortactin distributions revealed the complete overlap of the two proteins in all the cells (Fig. 7B and C, cor and act). Cortactin phosphorylation was elevated in SrcY527F-expressing osteoclasts, compared with control cells. However, podosome clusters in cells expressing Src251 contained very high levels of phosphocortactin (Fig. 6B and C, cor pY421/cor, respectively).

To directly probe the role of cortactin phosphorylation in

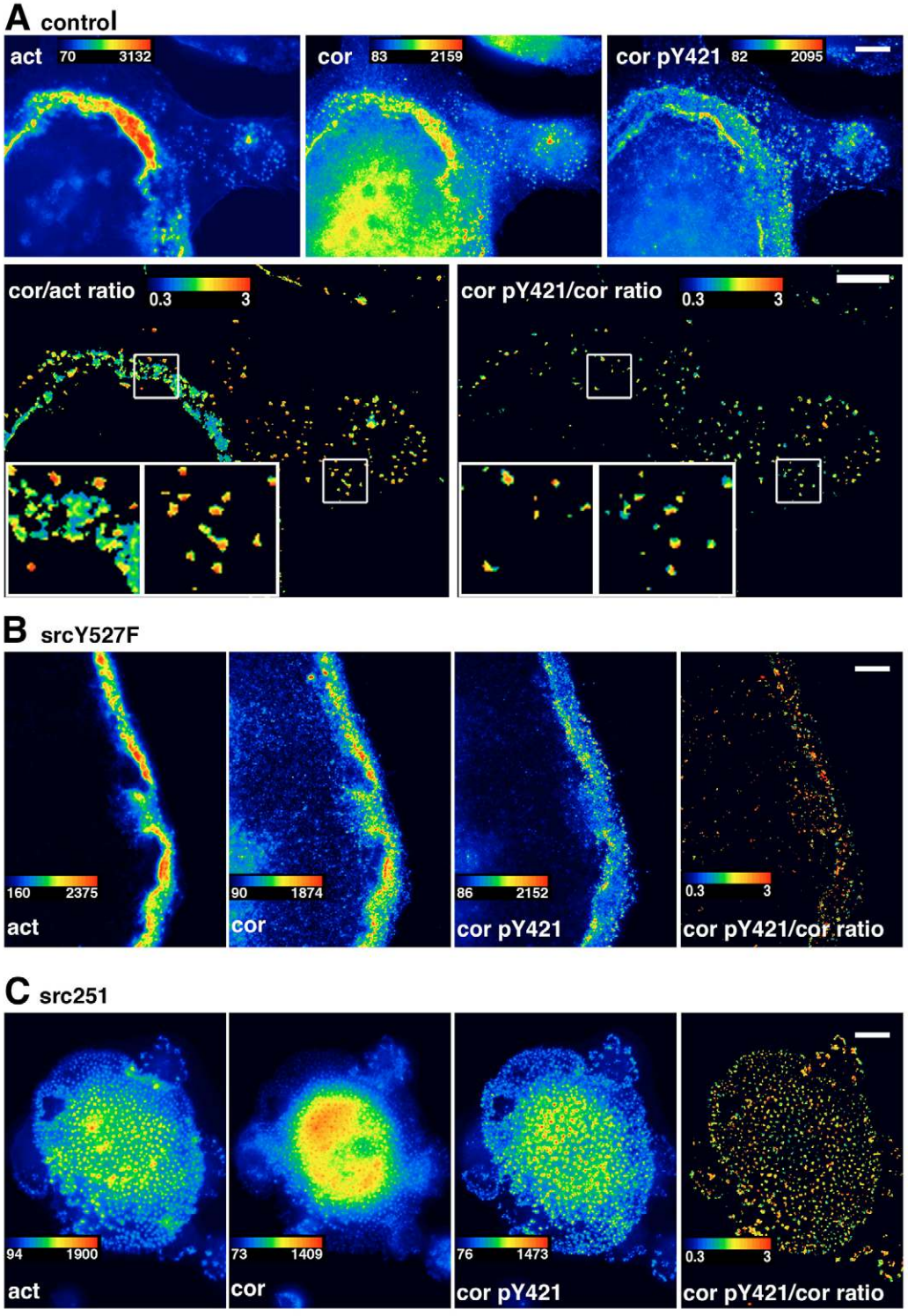

Fig. 7. Differential cortactin phosphorylation. (A) Control RAW osteoclasts, (B) cells co-expressing GFP-actin and SrcY527F, or (C) cells co-expressing GFP-actin and Src251 were fixed and triple-stained for actin (act), cortactin (cor) and phosphorylated cortactin (cor pY421). (A) Cortactin/actin ratio image highlights cortactin association with both SZL structure and clustered podosomes. Note the dramatic decrease in cortactin phosphorylation at the SZL structure (cor pY421/cor ratio image). (B) In SrcY527F-expressing cells, cortactin phosphorylation is moderately increased (cor pY421/cor ratio). (C) In Src251-expressing cells, cortactin is highly phosphorylated (cor pY421/cor ratio). Bars, 10 μm.

regulating podosome dynamics, we decided to overexpress a WT cortactin or a mutant molecule, in which the three tyrosine residues normally phosphorylated by Src (Y421, Y466 and Y482), were mutated to phenylalanine (cortactin-3YF) (Huang et al., 1998). Accordingly, we transfected RAW-derived osteoclasts with both constructs, and evaluated their localization to podosomes by co-staining for actin and the flag tag. Both constructs were localized to podosomes (Fig. 8A,B).

To evaluate the decrease in cortactin tyrosine phosphorylation, we used the water segmentation analysis to calculate the average intensity of both general and phosphorylated cortactin (cortactin pY421) specifically at the actin cores of clustered podosomes (Fig. 8C,D). In control cells (transfected with GFP-actin), cortactin was highly phosphorylated (Fig. 8C). The ratio between the intensities of phosphocortactin and general cortactin was 7 (Fig. 8D). Overexpression of WT or 3YF

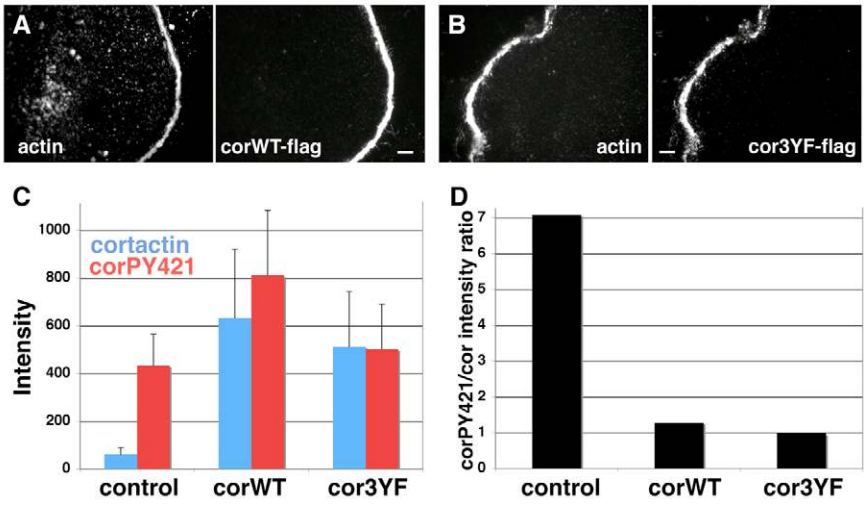

Fig. 8. Overexpression of cortactin mutants decreases cortactin phosphorylation in podosomes. RAW-derived osteoclasts were co-transfected with GFP-actin and corWT-flag or GFP-actin and cor3YF-flag. Cells were fixed and stained for the flag tag. (A) CorWT and (B) cor3YF localized to podosomes. (C) Cells were fixed and stained for cortactin and cortactin pY421. Five control cells, eight cells expressing corWT and eight cells expressing cor3YF were segmented and the fluorescence intensity of their podosomes was determined. In control cells, the average cortactin intensity calculated (±s.d.) was 61±27 (cortactin) and 432±132 (cortactin pY421). In cells overexpressing corWT, the average intensities calculated were 638±288 (cortactin) and 811±271 (cortactin pY421). In cells overexpressing cor3YF, the average cortactin intensity calculated (±s.d.) was 512±230 (cortactin) and 501±189 (cortactin pY421). Note the ten- or eightfold increase in cortactin intensity in cells expressing corWT or cor3YF, respectively, and only a 45% or 16% increase in cortactin phosphorylation in these cells. (D) The ratio of phosphocortactin to general cortactin intensities.

cortactin increased cortactin intensity at podosomes about tenfold (Fig. 8C). In cells overexpressing WT or 3YF cortactin, the ratios between the phosphorylated cortactin and the general protein were much smaller: 1.3 and 1, respectively (Fig. 8D). These changes in cortactin phosphorylation status are reminiscent of cortactin found at SZL structures (Fig. 7A).

To relate the decrease in cortactin phosphorylation to podosome dynamics, we transfected RAW-derived osteoclasts with GFP-actin and either WT cortactin or 3YF cortactin, and monitored podosome dynamics. In control cells transfected with GFP-actin and an empty dsRED vector, actin cores of clustered podosomes had an average life span of 169±107 seconds (Fig. 9A,B, control). Overexpression of WT cortactin significantly reduced the apparent podosome life span to 128±73 seconds ($P<5\times10^{-4}$) (Fig. 9A,B, corWT), whereas expression of the 3YF mutant shortened the actin life span to 84±54 seconds ($P<5\times10^{-13}$ both for control vs. cor3YF and corWT vs. cor3YF) (Fig. 9A,B, cor3YF). For statistical evaluation, see legend to Fig. 9.

We then examined the role of cortactin phosphorylation in podosome dynamics and osteoclast polarization by expressing WT or 3YF cortactin or with an empty dsRED vector as a control in Src251 osteoclasts. In control cells, large arrays of static podosomes were evident (Fig. 9C, control). In cells overexpressing WT or 3YF cortactin, podosome arrays were considerably smaller (Fig. 9C, corWT and cor3YF); furthermore, their actin cores were more dynamic than control podosomes. However, the increase in podosome dynamics did not lead to ring or SZL structure formation in these cells.

Discussion

The organization of podosomes and their assembly into superstructures such as clusters, rings and sealing zones, play a major role in regulating bone resorption by osteoclasts. In this study, we explored the involvement of Src and its substrate, cortactin, in podosome dynamics and maturation. We show herein that actin levels, as well as the rate of its reorganization, increase upon the transition of podosome clusters into rings, concomitantly with a decrease in the local levels of tyrosine-phosphorylated cortactin. In fully polarized cells, the dynamic reorganization of actin remains high whereas paxillin, associated with the same superstructure, is considerably more stable. This finding suggests that the Src-dependent phosphorylation of cortactin downregulates cortactin activity, thereby suppressing podosome turnover. This notion is strongly corroborated by the finding that overexpression of cortactin, mutated in its major Src-phosphorylation sites, enhances actin dynamics in clustered podosomes.

It is interesting to note that the increase in actin dynamics in cells expressing non-phophorylatable cortactin did not impair cluster development, nor did it induce the formation of rings and SZL structures in cells overexpressing a dominant-negative Src. This observation sheds new light on the relationship between local actin reorganization and podosome maturation during osteoclast polarization. Specifically, it indicates that although a reduction in podosome dynamics is incompatible with ring formation, induction of high podosome turnover by expressing the 3YF-cortactin mutant is insufficient for triggering ring formation. Thus, Src appears to play a dual role in regulating podosomes: a local, cortactin-dependent effect on actin dynamic reorganization, and a cortactin-independent effect on global reorganization of the podosomal system during osteoclast polarization.

The interplay between Src scaffolding activity and catalytic activity deserves further discussion. Previous studies have shown that Src catalytic activity is crucial for focal adhesion turnover in fibroblasts (Fincham and Frame, 1998; Webb et al., 2004) whereas the scaffolding activity, mediated by the N-terminal SH2 and SH3 domains, can rescue the ability of cells to adhere and spread in Src-deficient fibroblasts (Kaplan et al., 1995) (reviewed by Carragher and Frame, 2004). Furthermore, osteoclasts expressing kinase-defective Src manage to rescue the bone phenotype of Src-null mice (Schwartzberg et al., 1997). This finding suggests that the scaffolding activity provided by catalytically inactive Src is sufficient to rescue the bone phenotype in the context of a live animal.

By contrast, it was reported that osteoclast polarization and bone resorption in culture requires kinase activity (Miyazaki et

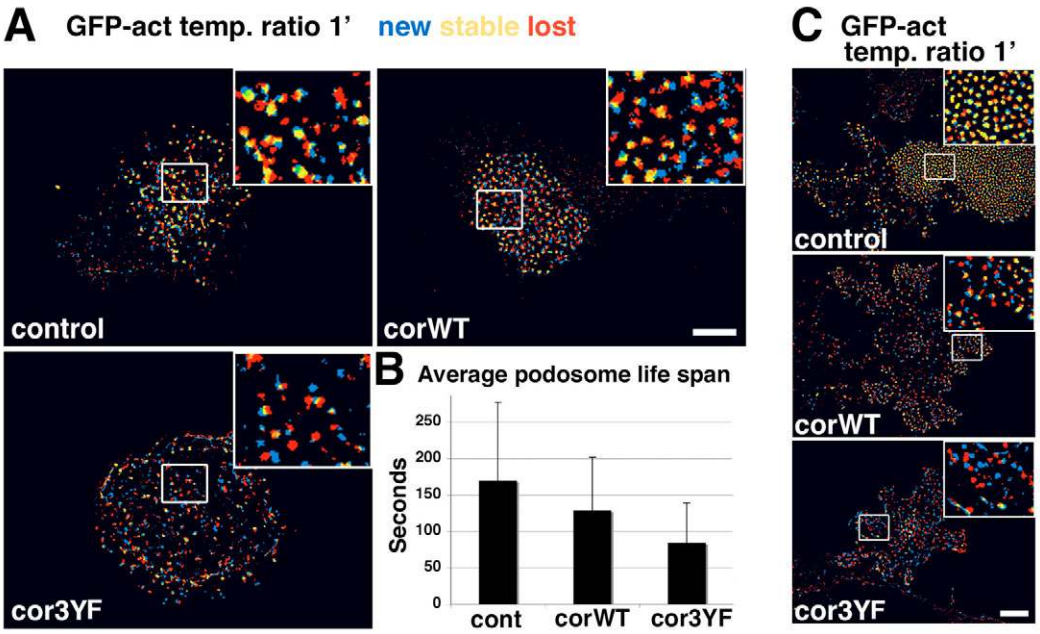

Fig. 9. Cortactin phosphorylation affects podosome dynamics. (A) RAW-derived osteoclasts were transfected with GFP-actin and dsRED (control), with GFP-actin and wild-type cortactin (corWT), or with GFP-actin and a cortactin phosphorylation mutant (cor3YF). Temporal ratio images, based on time-lapse microscopy of GFP-actin, are shown. Notice the decrease in stable podosomes in cells overexpressing either WT or mutant cortactin (corWT, cor3YF). (B) The calculated average (±s.d.) life span of cluster podosomes was 169±107 seconds in control cells, 128±73 seconds in cells overexpressing WT cortactin, and 84±54 seconds in cells overexpressing cortactin 3YF. For control cells, a total of 159 podosomes from four cells in three independent experiments were analyzed; for cells expressing WT cortactin, seven cells from three experiments, with a total of 238 podosomes were examined; for cortactin 3YF, nine cells from four experiments, with a total of 402 podosomes, were examined. Statistical differences were calculated using the Student's *t*-test (control vs. corWT cells: $P<5\times10^{-4}$; control vs. cor3YF, and corWT vs. cor3YF cells: $P<5\times10^{-13}$). (C) RAW cells co-expressing GFP-actin and Src251 were transfected with dsRED (control); dsRED and WT cortactin (corWT); or dsRED and cor3YF. Temporal ratio images based on time-lapse microscopy of GFP-actin are shown. Notice the increase in podosome dynamics without the development of rings or SZL structures, in cells overexpressing corWT and cor3YF. Bars, 10 μm.

al., 2004). The reasons for this apparent discrepancy between the in vivo and cell culture results are not clear. Our data, however, indicate that Src catalytic activity is crucial for at least three distinct processes associated with podosome development, namely: the proper assembly of the ring domain around the actin core (i.e. maturation of an individual podosome); regulation (via cortactin) of actin core dynamics; and the formation of podosome rings and, ultimately, a sealing zone. It should be emphasized that these Src-phosphorylation-driven processes require regulated Src activity; excessive, deregulated Src (e.g. the Src Y527F mutant) results in loss of normal structures, as a result of abnormally high podosome turnover.

The present study also highlights the role of cortactin in the regulation of podosome dynamics. Cortactin is an F-actin-binding protein that interacts with Arp2/3 (Uruno et al., 2001) and WASP/nWASP (Martinez-Quiles et al., 2004) to promote actin nucleation and polymerization (Wu et al., 1991; Uruno et al., 2001; Weed et al., 2000). It is thus not surprising that cortactin co-localizes with F-actin in peripheral extensions of many cell types (Wu et al., 1991), and in podosomes of all cell types, including osteoclasts, reported in the literature thus far (Hiura et al., 1995; Pfaff and Jurdic, 2001). Downregulating cortactin expression by siRNA prevents podosome formation in vascular smooth muscle cells (Zhou et al., 2005) and osteoclasts (Tehrani et al., 2006) suggesting a pivotal role for cortactin in podosome formation. It has been suggested that cortactin comes into play at an early stage of de novo podosome assembly (Tehrani et al., 2006; Webb et al., 2006). It is noteworthy that during osteoclast differentiation, cortactin levels increase 15-fold (Hiura et al., 1995), in line with the notion that cortactin-mediated actin rearrangement plays a pivotal role in osteoclasts.

A central issue in this report concerns the effect of cortactin phosphorylation by Src on actin dynamic reorganization in living cells. It was previously shown that Src-mediated cortactin phosphorylation makes it more susceptible to calpain degradation (Huang et al., 1997b), and decreases its ability to bind to F-actin (Huang et al., 1997a), and to activate WASP/nWASP (Martinez-Quiles et al., 2004). Here, we report that podosome structures with relatively high levels of phosphocortactin display low actin turnover, whereas areas enriched with non-phosphorylated cortactin are significantly more dynamic. These findings suggest that phosphorylation or dephosphorylation of cortactin can modulate podosome dynamics. This notion is further corroborated by the fact that overexpression of non-phosphorylatable cortactin considerably increases podosome dynamics. Recently, Tehrani et al. demonstrated that cortactin 3YF can localize to podosomes; however, it cannot substitute for the absence of endogenous, WT cortactin in osteoclasts (Tehrani et al., 2006). Taken together, these findings suggest that although high levels of phosphorylation are essential for the de novo assembly of a

podosome, low levels of phosphorylation are responsible for upregulating podosome dynamics.

It is well known that adhesion dynamics are regulated by a variety of signals, which result in specific, post-translational modifications in adhesion-related proteins that mediate adhesion assembly and turnover (Geiger and Bershadsky, 2002; Geiger et al., 2001). In osteoclasts expressing constitutively active Src, we could only trace a moderate increase in cortactin tyrosine phosphorylation, whereas podosomes were highly dynamic. This observation suggests that in these osteoclasts, podosome turnover is not mediated by cortactin; rather, other targets phosphorylated by Src induce podosome turnover in these cells. Indeed, the ability of constitutively active Src to increase adhesion turnover was evident in fibroblasts in which cortactin is not associated with the adhesion structures (Fincham and Frame, 1998).

On the other hand, in cells expressing dominate-negative Src, the overall phosphotyrosine of podosomes (data not shown) and, in particular, cortactin tyrosine-phosphorylation levels, were shown to be elevated. The same observation was made in different cell types expressing the same Src mutant (Kaplan et al., 1994). We can still not conclusively explain the observed results, but would like to propose a rather simple model, according to which the Src251 mutant binds to podosomes, recruits elevated levels of phospho-cortactin to these sites via its SH2 domain, and possibly interferes with cortactin dephosphorylation.

The mechanisms responsible for cortactin dephosphorylation during osteoclast polarization are still unknown. One possible candidate is the downregulation of Src [e.g. by activating c-Src kinase (CSK)] in the developing rings and in the SZL structure, or the activation of specific tyrosine phosphatases capable of downregulating cortactin phosphorylation. The latter possibility is in line with the observation that, in osteoclasts derived from osteopetrotic mice lacking protein tyrosine phosphatase ϵ (PTPϵ), normal podosome clusters fail to mature into rings and SZL structures (Chiusaroli et al., 2004). Further studies of local actin dynamics in different podosomal structures, in the presence of various polymerization modulators, may shed light on the mechanisms underlying the assembly of the resorptive apparatus. Such experiments are currently underway.

Materials and Methods

cDNA, reagents and antibodies

GFP-actin (Ballestrem et al., 1998), Cherry-actin was a generous gift from J. V. Small (Institute of Molecular Biology, Austrian Academy of Sciences, Salzburg, Austria), YFP-paxillin and GFP-paxillin vectors were constructed as described (Zamir et al., 2000). Cortactin WT and cortactin 3YF were prepared as previously described (Wu and Parsons, 1993; Wu et al., 1991). Src251, Src251R175L and SrcY527F were a generous gift from Harold Varmus (Sloan-Kettering Institute, Memorial Sloan-Kettering Cancer Center, New York, NY).

Primary antibodies used included: Monoclonal anti-PY, #4G10 (Upstate Biotechnology, Charlottesville, VA, USA); monoclonal anti-v-Src (Calbiochem, San Diego, CA), monoclonal anti-vinculin (clone hVin-1, Sigma, St Louis, MO, USA), monoclonal anti-cortactin (clone 4F11, Upstate, Waltham, MA) polyclonal anti-cortactin pY421, and polyclonal anti-Src pY418 (Biosource, Camarillo, CA). Secondary antibodies used were: donkey anti-rabbit IgG conjugated to Cy5, and donkey anti-mouse IgG conjugated to Cy3 (both showing minimal cross-reactivity with Ig of other species, for multi-labeling), and goat anti-mouse IgG conjugated to Cy3 (Jackson ImmunoResearch Laboratories, West Grove, PA). Actin was labeled with phalloidin conjugated to FITC (Sigma).

Cell culture, transfection, infection, fixation and staining

RAW 264.7 cells were obtained from the American Type Culture Collection (Manassas, VA). To induce osteoclast differentiation, 100 cells/mm^2 were grown at 37°C in a 5% CO_2 humidified atmosphere for 3 days in alpha MEM with Earle's salts, L-glutamine and $NaHCO_3$ (Sigma) supplemented with 10% fetal bovine serum (FBS) (Gibco, Grand Island, NY) and antibiotics (Biological Industries, Beit Haemek, Israel), 20ng/ml recombinant soluble receptor activator of NFκB ligand (RANK-L) and 20 ng/ml macrophage colony-stimulating factor (mCSF) (R&D, Minneapolis, MN). Primary osteoclasts were prepared as previously described (Chiusaroli et al., 2004).

Transfections (4 μg plasmid DNA per 3.5 cm plate) were conducted with lipofectamine 2000 (Invitrogen, Carlsbad, CA) after 48 hours of differentiation. Cells were then allowed to differentiate for an additional 30 hours and then assayed. For retroviral infection, 293T cells were transfected with CA10 Src251 or CA10SrcY527F vectors, 30, 40 and 50 hours after transfection. The media containing viruses were applied to GFP-actin-expressing RAW264.7 cells. The cells expressing the constructs were selected with hygromycin B (Calbiochem).

For staining, cells were fixed for 2 minutes in warm 3% paraformaldehyde (PFA) (Merck, Darmstadt, Germany) + 0.5% Triton X-100 (Sigma), and then in PFA alone for an additional 40 minutes. After fixation, cells were washed three times with PBS, pH 7.4, and incubated with primary antibody for 40 minutes, washed again three times in PBS, and incubated for an additional 40 minutes with secondary antibodies

Image acquisition and live cell imaging

Movies and fixed cell data were acquired with a DeltaVision system (Applied Precision, Issaquah, WA), consisting of an inverted microscope IX70 equipped with 60×/1.4 or 100×/1.3 objectives (Olympus, Tokyo, Japan) and with a temperature-controlled box (Life Imaging Services, Switzerland, www.lis.ch) using Resolve3D software (Applied Precision). For live cell imaging, RAW cells were induced to differentiate in 35 mm glass-bottomed, medium was then changed to DMEM containing 25 mM HEPES without Phenol Red and riboflavin (Biological Industries, Beit Haemek, Israel), and supplemented with 10 ng/ml mCSF and 10 ng/ml RANKL. 3D image reconstruction data were acquired by Zeiss LSM510 confocal microscopy (Zeiss, Oberkochen, Germany).

Image analysis and statistics

All image analyses were carried out using Priism software for Linux operating systems (http://msg.ucsf.edu/IVE/Download/). To calculate the average podosome life span, time-lapse movies of GFP-actin from at least three different osteoclast preparations were collected at intervals of 10, 15 or 30 seconds. Movies were high-pass filtered (Zamir et al., 1999) and podosomes were traced along the movies. The calculation of average podosome life span, in all types of structures was based on sampling of podosomes from all parts of the super-structure. In cases of podosome fission or fusion, the daughter podosome(s) were counted as new structures.

Temporal ratios, and ratios between components, were then produced, as previously described (Zamir et al., 1999). Briefly, the temporal ratio frame $t+x$ was divided by t to produce a 'spectral image' in which blue pixels indicated new positive pixels, red pixels indicated faded structures and the intermediate colors represented more stable structures. The ratio between components was calculated by dividing the fluorescence intensities of two components thereby yielding a spectrum of numerators values that varied between 0.1 to 10 or 0.3 to 3.

Autocorrelation analysis was performed on movies that were high-pass filtered, after determining a threshold above which all pixels were defined as parts of adhesion structures. A mask was created by all pixels above the threshold in the first frame. In each consecutive frame, the sum of intensities of all pixels within this mask was multiplied by the sum of intensities in the first frame. The resulting values were then normalized, so that the multiplication of the first frame by itself would equal one. This measure of autocorrelation takes into account both changes in intensity of an adhesion, and misalignment resulting from movement of an adhesion. As both phenomena are indicative of disassembly, we view this autocorrelation index as an indicator of adhesion dynamics.

Measurements of podosome number and average intensity were performed by segmenting the images, using the so-called 'water algorithm', as previously described (Zamir et al., 1999).

We would like to thank Christoph Ballestrem for his help with live cell imaging, Zvi Kam for his assistance with image analysis and data interpretation, Alexander Bershadsky for illuminating discussions, and Ari Elson for fruitful comments and careful reading of the manuscript. Shira Granot-Attas and Yulya Zilberman for their assistance. B.G. holds the Erwin Neter Professorial Chair in Cell and Tumor Biology. L.A. holds the Dorothy and Patrick E. Gorman Professorial Chair of Biological Ultrastructure. This study was supported by NIGMS, National Institutes of Health Cell Migration Consortium Grant U54 GM64346 and the United States-Israel Binational Science Foundation (to B.G.)

References

Ballestrem, C., Wehrle-Haller, B. and Imhof, B. A. (1998). Actin dynamics in living mammalian cells. *J. Cell Sci.* **111**, 1649-1658.

Calle, Y., Jones, G. E., Jagger, C., Fuller, K., Blundell, M. P., Chow, J., Chambers, T. and Thrasher, A. J. (2004). WASp deficiency in mice results in failure to form osteoclast sealing zones and defects in bone resorption. *Blood* **103**, 3552-3561.

Carragher, N. O. and Frame, M. C. (2004). Focal adhesion and actin dynamics: a place where kinases and proteases meet to promote invasion. *Trends Cell Biol.* **14**, 241-249.

Chellaiah, M., Kizer, N., Silva, M., Alvarez, U., Kwiatkowski, D. and Hruska, K. A. (2000). Gelsolin deficiency blocks podosome assembly and produces increased bone mass and strength. *J. Cell Biol.* **148**, 665-678.

Chiusaroli, R., Knobler, H., Luxenburg, C., Sanjay, A., Granot-Attas, S., Tiran, Z., Miyazaki, T., Harmelin, A., Baron, R. and Elson, A. (2004). Tyrosine phosphatase epsilon is a positive regulator of osteoclast function in vitro and in vivo. *Mol. Biol. Cell* **15**, 234-244.

Destaing, O., Saltel, F., Geminard, J. C., Jurdic, P. and Bard, F. (2003). Podosomes display actin turnover and dynamic self-organization in osteoclasts expressing actin-green fluorescent protein. *Mol. Biol. Cell* **14**, 407-416.

Evans, J. G., Correia, I., Krasavina, O., Watson, N. and Matsudaira, P. (2003). Macrophage podosomes assemble at the leading lamella by growth and fragmentation. *J. Cell Biol.* **161**, 697-705.

Fincham, V. J. and Frame, M. C. (1998). The catalytic activity of Src is dispensable for translocation to focal adhesions but controls the turnover of these structures during cell motility. *EMBO J.* **17**, 81-92.

Geiger, B. and Bershadsky, A. (2002). Exploring the neighborhood: adhesion-coupled cell mechanosensors. *Cell* **110**, 139-142.

Geiger, B., Bershadsky, A., Pankov, R. and Yamada, K. M. (2001). Transmembrane crosstalk between the extracellular matrix–cytoskeleton crosstalk. *Nat. Rev. Mol. Cell Biol.* **2**, 793-805.

Head, J. A., Jiang, D., Li, M., Zorn, L. J., Schaefer, E. M., Parsons, J. T. and Weed, S. A. (2003). Cortactin tyrosine phosphorylation requires Rac1 activity and association with the cortical actin cytoskeleton. *Mol. Biol. Cell* **14**, 3216-3229.

Hiura, K., Lim, S. S., Little, S. P., Lin, S. and Sato, M. (1995). Differentiation dependent expression of tensin and cortactin in chicken osteoclasts. *Cell Motil. Cytoskeleton* **30**, 272-284.

Horne, W. C., Neff, L., Chatterjee, D., Lomri, A., Levy, J. B. and Baron, R. (1992). Osteoclasts express high levels of pp60c-src in association with intracellular membranes. *J. Cell Biol.* **119**, 1003-1013.

Huang, C., Ni, Y., Wang, T., Gao, Y., Haudenschild, C. C. and Zhan, X. (1997a). Down-regulation of the filamentous actin cross-linking activity of cortactin by Src-mediated tyrosine phosphorylation. *J. Biol. Chem.* **272**, 13911-13915.

Huang, C., Tandon, N. N., Greco, N. J., Ni, Y., Wang, T. and Zhan, X. (1997b). Proteolysis of platelet cortactin by calpain. *J. Biol. Chem.* **272**, 19248-19252.

Huang, C., Liu, J., Haudenschild, C. C. and Zhan, X. (1998). The role of tyrosine phosphorylation of cortactin in the locomotion of endothelial cells. *J. Biol. Chem.* **273**, 25770-25776.

Hurst, I. R., Zuo, J., Jiang, J. and Holliday, L. S. (2004). Actin-related protein 2/3 complex is required for actin ring formation. *J. Bone Miner. Res.* **19**, 499-506.

Kaplan, K. B., Bibbins, K. B., Swedlow, J. R., Arnaud, M., Morgan, D. O. and Varmus, H. E. (1994). Association of the amino-terminal half of c-Src with focal adhesions alters their properties and is regulated by phosphorylation of tyrosine 527. *EMBO J.* **13**, 4745-4756.

Kaplan, K. B., Swedlow, J. R., Morgan, D. O. and Varmus, H. E. (1995). c-Src enhances the spreading of src–/– fibroblasts on fibronectin by a kinase-independent mechanism. *Genes Dev.* **9**, 1505-1517.

Lakkakorpi, P. T., Helfrich, M. H., Horton, M. A. and Vaananen, H. K. (1993). Spatial organization of microfilaments and vitronectin receptor, alpha v beta 3, in osteoclasts. A study using confocal laser scanning microscopy. *J. Cell Sci.* **104**, 663-670.

Lakkakorpi, P. T., Nakamura, I., Young, M., Lipfert, L., Rodan, G. A. and Duong, L. T. (2001). Abnormal localisation and hyperclustering of (alpha)(V)(beta)(3) integrins and associated proteins in Src-deficient or tyrphostin A9-treated osteoclasts. *J. Cell Sci.* **114**, 149-160.

Linder, S. and Aepfelbacher, M. (2003). Podosomes: adhesion hot-spots of invasive cells. *Trends Cell Biol.* **13**, 376-385.

Luxenburg, C., Addadi, L. and Geiger, B. (2006). The molecular dynamics of osteoclast adhesions. *Eur. J. Cell Biol.* **85**, 203-211.

Martinez-Quiles, N., Ho, H. Y., Kirschner, M. W., Ramesh, N. and Geha, R. S. (2004). Erk/Src phosphorylation of cortactin acts as a switch on-switch off mechanism that controls its ability to activate N-WASP. *Mol. Cell. Biol.* **24**, 5269-5280.

Miyazaki, T., Sanjay, A., Neff, L., Tanaka, S., Horne, W. C. and Baron, R. (2004). Src kinase activity is essential for osteoclast function. *J. Biol. Chem.* **279**, 17660-17666.

Nesbitt, S. A. and Horton, M. A. (1997). Trafficking of matrix collagens through bone-resorbing osteoclasts. *Science* **276**, 266-269.

Ochoa, G. C., Slepnev, V. I., Neff, L., Ringstad, N., Takei, K., Daniell, L., Kim, W., Cao, H., McNiven, M., Baron, R. et al. (2000). A functional link between dynamin and the actin cytoskeleton at podosomes. *J. Cell Biol.* **150**, 377-389.

Pfaff, M. and Jurdic, P. (2001). Podosomes in osteoclast-like cells: structural analysis and cooperative roles of paxillin, proline-rich tyrosine kinase 2 (Pyk2) and integrin alphaVbeta3. *J. Cell Sci.* **114**, 2775-2786.

Salo, J., Lehenkari, P., Mulari, M., Metsikko, K. and Vaananen, H. K. (1997). Removal of osteoclast bone resorption products by transcytosis. *Science* **276**, 270-273.

Sanjay, A., Houghton, A., Neff, L., DiDomenico, E., Bardelay, C., Antoine, E., Levy, J., Gailit, J., Bowtell, D., Horne, W. C. et al. (2001). Cbl associates with Pyk2 and Src to regulate Src kinase activity, alpha(v)beta(3) integrin-mediated signaling, cell adhesion, and osteoclast motility. *J. Cell Biol.* **152**, 181-195.

Schwartzberg, P. L., Xing, L., Hoffmann, O., Lowell, C. A., Garrett, L., Boyce, B. F. and Varmus, H. E. (1997). Rescue of osteoclast function by transgenic expression of kinase-deficient Src in src–/– mutant mice. *Genes Dev.* **11**, 2835-2844.

Soriano, P., Montgomery, C., Geske, R. and Bradley, A. (1991). Targeted disruption of the c-src proto-oncogene leads to osteopetrosis in mice. *Cell* **64**, 693-702.

Tarone, G., Cirillo, D., Giancotti, F. G., Comoglio, P. M. and Marchisio, P. C. (1985). Rous sarcoma virus-transformed fibroblasts adhere primarily at discrete protrusions of the ventral membrane called podosomes. *Exp. Cell Res.* **159**, 141-157.

Tehrani, S., Faccio, R., Chandrasekar, I., Ross, F. P. and Cooper, J. A. (2006). Cortactin has an essential and specific role in osteoclast actin assembly. *Mol. Biol. Cell* **7**, 2882-2895.

Teitelbaum, S. L. (2000). Bone resorption by osteoclasts. *Science* **289**, 1504-1508.

Uruno, T., Liu, J., Zhang, P., Fan, Y., Egile, C., Li, R., Mueller, S. C. and Zhan, X. (2001). Activation of Arp2/3 complex-mediated actin polymerization by cortactin. *Nat. Cell Biol.* **3**, 259-266.

Webb, B. A., Eves, R. and Mak, A. S. (2006). Cortactin regulates podosome formation: roles of the protein interaction domains. *Exp. Cell Res.* **312**, 760-769.

Webb, D. J., Donais, K., Whitmore, L. A., Thomas, S. M., Turner, C. E., Parsons, J. T. and Horwitz, A. F. (2004). FAK-Src signalling through paxillin, ERK and MLCK regulates adhesion disassembly. *Nat. Cell Biol.* **6**, 154-161.

Weed, S. A., Karginov, A. V., Schafer, D. A., Weaver, A. M., Kinley, A. W., Cooper, J. A. and Parsons, J. T. (2000). Cortactin localization to sites of actin assembly in lamellipodia requires interactions with F-actin and the Arp2/3 complex. *J. Cell Biol.* **151**, 29-40.

Wu, H. and Parsons, J. T. (1993). Cortactin, an 80/85-kilodalton pp60src substrate, is a filamentous actin-binding protein enriched in the cell cortex. *J. Cell Biol.* **120**, 1417-1426.

Wu, H., Reynolds, A. B., Kanner, S. B., Vines, R. R. and Parsons, J. T. (1991). Identification and characterization of a novel cytoskeleton-associated pp60src substrate. *Mol. Cell. Biol.* **11**, 5113-5124.

Zambonin-Zallone, A., Teti, A., Carano, A. and Marchisio, P. C. (1988). The distribution of podosomes in osteoclasts cultured on bone laminae: effect of retinol. *J. Bone Miner. Res.* **3**, 517-523.

Zambonin-Zallone, A., Teti, A., Grano, M., Rubinacci, A., Abbadini, M., Gaboli, M. and Marchisio, P. C. (1989). Immunocytochemical distribution of extracellular matrix receptors in human osteoclasts: a beta 3 integrin is colocalized with vinculin and talin in the podosomes of osteoclastoma giant cells. *Exp. Cell Res.* **182**, 645-652.

Zamir, E., Katz, B. Z., Aota, S., Yamada, K. M., Geiger, B. and Kam, Z. (1999). Molecular diversity of cell-matrix adhesions. *J. Cell Sci.* **112**, 1655-1669.

Zamir, E., Katz, M., Posen, Y., Erez, N., Yamada, K. M., Katz, B. Z., Lin, S., Lin, D. C., Bershadsky, A., Kam, Z. et al. (2000). Dynamics and segregation of cell-matrix adhesions in cultured fibroblasts. *Nat. Cell Biol.* **2**, 191-196.

Zhou, S., Webb, B. A., Eves, R. and Mak, A. S. (2005). Effects of Tyr-phosphorylation of cortactin on podosome-formation in A7r5 vascular smooth muscle cells. *Am. J. Physiol. Cell Physiol.* **290**, C463-C471.